Osteoarthritis-associated basic calcium phosphate crystals alter immune cell metabolism and promote M1 macrophage polarization.

Olwyn R. Mahon[1,2], Daniel J. Kelly[2,3], Geraldine, M. McCarthy[4] and Aisling Dunne[1,3,5]*.

[1] School of Biochemistry and Immunology, Trinity College Dublin, Dublin, Ireland. [2] Trinity Centre for Bioengineering, Trinity Biomedical Sciences Institute, Trinity College Dublin, Dublin, Ireland. [3] Advanced Materials and Bioengineering Research (AMBER) Centre, Trinity College Dublin, Ireland. [4]School of Medicine and Medical Science, University College Dublin and Misericordiae University Hospital, Dublin, Ireland Eccles Street, Dublin 1, Ireland. [5] School of Medicine, Trinity College Dublin, Dublin, Ireland.

Address correspondence to Aisling Dunne, School of Biochemistry & Immunology and School of Medicine, Trinity Biomedical Sciences Institute, Trinity College Dublin, Ireland. Email: aidunne@tcd.ie. Ph: +353-1-8962437.

Running title: BCP crystals drive immune cell metabolic reprogramming.

Abstract

Objective: A number of studies have demonstrated that molecules called 'alarmins' or danger-associated molecular patterns (DAMPs), contribute to inflammatory processes in the OA joint. Metabolic reprogramming of immune cells, including macrophages, is emerging as a prominent player in determining immune cell phenotype and function. The aim of this study was to investigate if basic calcium phosphate (BCP) crystals which are OA-associated DAMPs, impact on macrophage phenotype and metabolism.

Methods: Human monocyte derived macrophages were treated with BCP crystals and expression of M1 (CXCL9, CXCL10) and M2 (MRC1, CCL13)-associated markers was assessed by real-time PCR while surface maturation marker (CD40, CD80 & CD86) expression was assessed by flow cytometry. BCP induced metabolic changes were assessed by Seahorse analysis and glycolytic marker expression (hexokinase 2(HK2), Glut1 and HIF1α) was examined using real-time PCR and immunoblotting.

Results: Treatment with BCP crystals upregulated mRNA levels of CXCL9 and CXCL10 while concomitantly downregulating expression of CCL13 and MRC1. Furthermore, BCP-treated macrophages enhanced surface expression of the maturation makers, CD40, CD80 and CD86. BCP-treated cells also exhibited a shift towards glycolysis as evidenced by an increased ECAR/OCR ratio and enhanced expression of the glycolytic markers, HK2, Glut1 and HIF1α. Finally, BCP-induced macrophage activation and alarmin expression was reduced in the presence of the glycolytic inhibitor, 2-DG.

Conclusions: This study not only provides further insight into how OA-associated DAMPs impact on immune cell function, but also highlights metabolic reprogramming as a potential therapeutic target for calcium crystal-related arthropathies.

Introduction

Osteoarthritis (OA) is the most common form of chronic arthropathy and leading cause of disability worldwide. It affects 10% of males and 18% of females over the age of 45, a figure that is set to rise as life expectancy increases (1, 2). In addition, the current obesity epidemic has resulted in an increased incidence of OA in younger individuals, many of whom will undergo multiple joint replacements due to the limited lifespan of artificial joints. Extensive research has highlighted a complex interplay between chondrocytes, synovial fibroblasts and the innate immune network and while much progress has been made in elucidating the cellular and molecular events contributing to OA, the complex nature of the disease has hampered the development of a successful disease-modifying drug. Current therapies are focused on providing symptomatic relief rather than halting or reversing disease progression, hence, there is a clear need to identify specific orchestrators that initiate and/or contribute to eventual joint destruction.

Immunometabolism is an emerging field of research that focuses on changes in intracellular metabolic pathways in immune cells and how these alterations impact on cell fate and function (3–5). It is now recognised that a metabolic shift from oxidative phosphorylation to a highly metabolically active glycolytic state (designed to maintain energy homeostasis under conditions of low oxygen and acute stress) can lead to an accumulation of reactive oxygen species (ROS) and metabolic intermediates that promote the synthesis of degradative enzymes and inflammatory mediators (6). Increased glycolytic rates and glucose consumption are associated with enhanced expression of the glucose transporter, GLUT1, as well as elevated lactate production (7). Furthermore, activated immune cells exhibit Warburg metabolism and HIF-1α induction even under normoxic conditions (8, 9). Recent

studies have also demonstrated that macrophage activation and phenotype is intricately linked to cellular metabolic status. For example, lipopolysaccharide (LPS) activated M1 macrophages [M1(LPS)] exhibit an enhanced glycolytic profile characterised by increased expression of glucose transporters, glycolytic enzymes and rapid production of ATP (3, 10, 11). While this metabolic switch is required to meet the energy demands of the cell during infection and provide biosynthetic components required to carry out effector functions, dysregulated immune-cell metabolism which results in sustained inflammatory responses, has been linked to a number of debilitating diseases and it has been strongly suggested that strategies to modulate metabolic reprogramming represents a novel approach to regulate disease pathology (12–15). Furthermore, a number of metabolites have been shown to alter macrophage polarization and there is now a host of studies demonstrating how inhibitors of metabolism (e.g. glycolysis, fatty acid synthesis and fatty acid oxidation) can regulate immune responses providing potential new avenues to manipulate immune cell activation (15).

Altered immunometabolism has been recognised as a component of a number of inflammatory and autoimmune conditions (13–17) and while it is well established that glycolysis is important for energy production in chondrocytes, there is now also evidence for increased glycolysis and deregulated cellular metabolism in OA (18–21). Indeed, mitochondrial dysfunction is a hallmark of OA and previous studies have shown increased mitochondrial DNA damage in OA chondrocytes compared to healthy controls suggesting that cartilage degradation during OA and normal cartilage aging may be metabolically different processes (22). Furthermore, lactate levels are elevated in OA and are frequently co-associated with crystal arthropathy comorbidities (23, 24). Indeed, one notable link between mechanical and inflammatory mechanisms in OA pathogenesis is calcium crystal deposition. Basic calcium phosphate (BCP) crystals, comprised mainly of hydroxyapatite, are uniquely

associated with OA and have been identified in 100% of cartilage and 50% of synovial fluid samples at the time of joint replacement where their concentration correlates with the severity of histological and radiographic OA (25). Crystal deposition and articular calcification occurs as a result of dysregulated ossification processes and an imbalance between pro-mineralization and anti-mineralization factors. Direct injection of BCP-crystals into mouse knees results in synovial inflammation, cartilage destruction and chondrocyte apoptosis (26). As a result, these crystals are now considered damage-associated molecular patterns (DAMPs) or 'alarmins' as they can activate fibroblasts, macrophages and chondrocytes through a variety of signaling pathways which, in turn, leads to the production of inflammatory and catabolic mediators (27–32). While several pathological cellular mechanisms have been identified, studies examining the effects of BCP crystals in humans are lacking as are drugs that prevent crystal deposition, permit crystal dissolution or specifically target the pathogenic effects that result in clinical manifestations. In this study we demonstrate that BCP crystals polarize primary human macrophages towards an M1-like phenotype and upregulate the expression of glycolytic markers. This is accompanied by a bioenergetics switch in favour of glycolysis. Furthermore, we demonstrate that targeting glycolysis reduces BCP-induced macrophage polarization and alarmin expression, suggesting that calcium crystal deposition impacts on immune cell metabolic reprogramming and subsequent macrophage phenotype and function.

Methods

Reagents and assessment of endotoxin contamination in BCP preparations are described in supplementary methods.

Human blood monocyte-derived macrophage isolation

This study was approved by the research ethics committee of the School of Biochemistry and Immunology, Trinity College Dublin and was conducted in accordance with the Declaration of Helsinki. Leucocyte-enriched buffy coats from anonymous healthy donors were obtained with permission from the Irish Blood Transfusion Board (IBTS), St. James's Hospital, Dublin. Donors provided informed written consent to the IBTS for their blood to be used for research purposes. PBMC were isolated and differentiated into macrophages as described previously (33). The purity of $CD14^+CD11b^+$ macrophages was assessed by flow cytometry and was routinely >95% (Fig. S1).

Cytokine measurements

Cells were pre-treated with (PD98059 (20μM), SB203580 (20μM), for 45 min prior to stimulation with BCP crystals (50 μg/ml) for 24 hours. Supernatants were harvested and cytokine concentrations of TNFα, IL-6 and IL-8 were quantified by ELISA (eBioscience, San Diego, CA) according to manufacturer's protocol.

Real-time PCR

Macrophages were treated with BCP crystals (50 ug/ml) alone or in the presence of indicated inhibitors (PD98059 (20μM), SB203580 (20μM), Latrunculin B (1μM), Cytochalsin D (5 μM), Cytochalsin B (5 μM), Dynasore (80 μM) or 2-DG (25 mM). RNA was extracted using High-Pure RNA Isolation Kits (Roche), and assessed for concentration and purity using the NanoDrop

2000c UV–Vis spectrophotometer. RNA was equalised and reverse transcribed using the Applied Biosystems High-Capacity cDNA reverse transcription kit. Real-time PCR carried out on triplicate cDNA samples using the CFX96 Touch Real-Time PCR Detection System (Bio-Rad Laboratories, California). Reactions included iTaq Universal SYBR Green Supermix (Bio-rad Laboratories), cDNA, TaqMan fast universal PCR Master Mix and pre-designed TaqMan gene expression probes (Applied Biosystems) for CXCL9, CXCL10, MRC1, CCL13, S100A8 and the housekeeping gene, 18S ribosomal RNA. The $2-\Delta\Delta CT$ method was used to analyse relative gene expression. Oligonuceotide primer sequences for SYBR primers for HK2, Glut1, HIF1a, HIF2, GAPDH and HRPTL are provided in Supplementary Table 1.

Immunoblotting

Primary macrophages were stimulated BCP crystals (50 μg/ml) for 3, 6, or 24 hours for the detection Hexokinase 2 (HK2), Glut1 or HIF1α protein. Cells were lysed by addition of RIPA buffer (Tris 50 mM; NaCl 150 mM; SDS 0.1%; sodium deoxycholate 0.5%; Triton X 100). Lysates were electrophoresed on SDS-PAGE gels (12% gel for Glut1, 10% gel for HK2 and 7.5% gel for HIF1α) and transferred to PVDF membranes (Millipore, Massachusetts) prior to detection with anti-HK2 or anti-Glut1 antibodies (Supplementary Table 2).

Flow cytometry

Primary human macrophages were plated at a concentration of 1 x 10^6 cells/ml and stimulated with BCP crystals (50 μg/ml) for 24 hours in the absence or presence of the glycolytic inhibitor 2-DG (25 mM). Cells were collected, washed, Fcγ blocked and stained extracellularly with amine-binding markers for dead cells (Fixable Viability Dye; eBioscience) for 10 minutes. Cells were washed in PBS and stained with fluorochrome-conjugated

antibodies specific for CD14, CD11b, CD86, CD40 and CD80 (all eBiosciences) and fixed with 2% paraformaldehyde (PFA) washed and acquired. The model antigen DQ-Ova, which fluoresces upon processing by proteases inside the cell, was used to assess phagocytic capacity of the cells. Macrophages were cultured with complete RPMI containing DQ-Ovalbumin (500 ng/ml; Invitrogen) for 20 minutes at 37 °C, followed by incubation for 10 minutes at 4 °C. Cells were then washed in PBS and immediately acquired. Cells were acquired on a FACSCanto TM II (BD Biosciences) and analysis was performed with FlowJo v.10 so ware (Tree Star Inc.). Gating strategies utilised in all experiments are detailed in Supplementary Figure 1.

Seahorse Analyser

Macrophages were cultured at 1 x 10 6 cells/ml for 6 days prior to re-seeding at 2 × 10^5 cells/well in a Seahorse 96-well microplate and allowed to rest for 5 hours prior to BCP or LPS stimulation. The Seahorse cartridge plate was hydrated with XF calibrant fluid and incubated in a non-CO_2 incubator at 37°C for a minimum of 8 h prior to use. To determine the effect of BCP crystals, macrophages were incubated with BCP crystals (50 ug/ml) for 24 h, prior to analysis using a Seahorse XFe24 analyser. 30 min prior to placement into the XF/XFe analyser, cell culture medium was replaced with complete XF assay medium (Seahorse Biosciences; supplemented with 10 mM glucose, 1 mM sodium pyruvate, 2 mM L-glutamine, and pH adjusted to 7.4) and incubated in a non-CO_2 incubator at 37°C. Blank wells (XF assay medium only) were prepared without cells for subtracting the background oxygen consumption rate (OCR) and extracellular acidification rate (ECAR) during analysis. Oligomycin (1µM; Cayman Chemicals), carbonyl cyanide-p-trifluoromethoxyphenylhydrazone (FCCP) (1µM; Santa Cruz biotechnology), rotenone (500 nM), and antimycin A (500 nM) and 2-deoxy-

D-glucose (2-DG) (25mM; all Sigma-Aldrich) were prepared in XF assay medium and loaded into the appropriate injection ports on the cartridge plate and incubated for 10 min in a non-CO_2 incubator at 37°C. OCR and ECAR were measured over time with sequential injections of oligomycin, FCCP, rotenone and antimycin A and 2-DG. Analysis of results was performed using Wave software (Agilent Technologies). The rates of basal glycolysis, max glycolysis, glycolytic reserve etc. were calculated as detailed in the manufacturer's protocol and supplied in Supplementary Table 3.

Statistical Analysis

Each experiment was performed in at least 4 healthy donors (defined by N) with 3-4 technical replicates run for each experiment, (defined by *n*) depending on the assay type. Paired one-way ANOVA or Kruskal-Wallis tests were used for the comparison of more than two groups for parametric and non-parametric analysis respectively, with the Tukey or Dunn's post-test (where applicable). A paired Student's t-test was used when there were only two groups for analysis and the data was normally distributed and a Two-tailed paired Wilcoxon Signed rank test was used for non-parametric data. All statistical analysis was performed on GraphPad Prism 7.00 (GraphPad Software). *P* value <0.05 were deemed significant.

Results:

BCP crystals promote M1 macrophage polarization.

We and others have previously reported that BCP-crystals drive inflammatory mediator and alarmin production in macrophages, fibroblasts and chondrocytes (27, 29, 32). In order to determine if BCP crystals impact on macrophage polarization, primary human macrophages were treated with previously published doses of BCP crystals (50 μg/ml) for 24 hours and expression of established genes associated with M(LPS) (i.e. prototypic M1-like MDMs) and M(IL-4) (i.e. prototypic M2-like MDMs) macrophage polarization was assessed by real-time PCR. While BCP stimulation of macrophages significantly enhanced the mRNA expression of the M(LPS) markers, CXCL9 and CXCL10, compared to control samples, treatment of macrophages with the crystals led to a significant decrease in basal levels of the M(IL-4) macrophage markers, MRC1 and CCL13 [Fig. 1(A-D)]. Furthermore, treatment of macrophages with BCP crystals significantly enhanced secretion of the chemokine, IL-8 [Fig. 1 (E)]. Treatment of macrophages with BCP-crystals did not induce secretion of the cytokines TNFα or IL-6 (Fig. S2A) which is in agreement with published results examining BCP-induced responses in macrophages (30) and together with results from the HEK-Blue^{TM} hTLR4 assay system (Invivogen) (Fig. S2B) signifies a lack of endotoxin contamination in our BCP crystal preparation.

We have previously demonstrated that BCP crystals activate MAPKs downstream of Syk in a receptor independent manner (29, 30). Pre-treatment of macrophages with either SB203580 or PD98059 to inhibit p38 and ERK, respectively, significantly inhibited BCP-induced IL-8, CXCL9 and CXCL10 expression [Fig. 1 (F-H)], demonstrating that MAPK activation is also involved BCP-induced macrophage polarization. Of note, inhibition of MAPKs had no effect

on MRC1 or CCL13 mRNA expression in BCP treated macrophages (Fig. S3). In addition to CXCL9/10 expression, we assessed surface expression of the M1-associated maturation markers, CD86, CD80, CD40 [Fig. 1 (I & J)]. BCP crystals stimulation induced a significant increase in the expression of CD86 and CD40, and although not significant, a trend towards increased CD80 surface marker expression was also observed (p=0.0674). Finally, the phagocytic capacity of macrophages was assessed following BCP stimulation given that activated M1-like macrophages reduce their phagocytic capacity upon activation (34). Cells were incubated with FITC-conjugated DQ-Ovalbumin (DQ-Ova) at 500 ng/ml post BCP stimulation and analysed for antigen uptake by flow cytometry. As expected, unstimulated macrophages exhibited high DQ-Ova uptake, however, this was significantly reduced upon stimulation of cells with BCP crystals [Fig. 1 (K & L].

BCP crystals alter macrophage metabolism and promote glycolysis.

A number of studies have demonstrated that activated macrophages exhibit an enhanced glycolytic profile characterised by increased expression of glucose transporters and glycolytic enzymes (35). In order to determine whether BCP crystal-induced macrophage polarization coincided with a metabolic switch favoring glycolysis, macrophages were treated with BCP and established markers of glycolysis were assessed by real-time PCR and immunoblotting. BCP crystals significantly upregulated mRNA expression of the glucose transporter, GLUT 1 the glycolytic enzyme, hexokinase 2 (HK2) and the transcription factor, HIF1α. There was also a trend towards increased expression of glyceraldehyde-3-phosphate dehydrogenase (GAPDH) (p=0.0634), [Fig. 2 (A)]. No difference in mRNA expression of HIF2α was observed (Fig. S4). Furthermore, protein levels of both HK2 and GLUT1 and were found to be highly expressed at 24 hours post BCP crystal treatment, while increased expression of HIF1α was

observed at 3, 6 and 24 hours post stimulation [Fig. 2 (B)]. Densitometric analysis revealed a dose dependent upregulation of HK2 and Glut 1 proteins at 3, 6 and 24 hours with maximal and significant upregulation occurring at 24 hours for both proteins [Fig. 2 (C)]. To further investigate whether BCP treated cells were altering their energy metabolism to a more glycolytic state, we measured both glycolysis and oxidative phosphorylation using the Seahorse XF-Analyzer. Macrophages were seeded into a Seahorse microplate and stimulated with BCP crystals for 3, 6 or 24 hrs. The rates of glycolysis and oxidative phosphorylation were determined by the measurement of ECAR (extracellular acidification rate) and OCR (oxygen consumption rate), respectively, before and after injections of oligomycin, FCCP, rotenone, antimycin A and 2-DG. Overall, the ECAR of BCP-treated cells was higher than untreated controls with the highest ECAR observed at 3 hours post-stimulation [Fig. 2 (D)]. The basal rate of glycolysis was increased in BCP-treated macrophages at all time points, compared to that of untreated control cells [Fig. 2 (G)], while the maximum rate of glycolysis, was also enhanced in BCP stimulated cells, peaking at 3 hours [Fig. 3 (H)]. The respiratory profiles of macrophages appeared to mirror their observed glycolytic activity with 3 and 6 hour BCP stimulation inducing the highest OCR, while 24 hour stimulation appeared to marginally reduce OCR [Fig 2 (E)]. This was reflected in the calculated basal respiration and max respiration (Fig. S5). Importantly, the ECAR:OCR ratio was increased in BCP treated cells at all time points tested [Fig. 2 (I)]. We also compared the metabolic profile of BCP-treated cells to that of a known PAMP, LPS which was marginally more potent than BCP at driving CXCL9 and CXCL10 gene expression (Fig. S6I & J). While both treatments enhanced glycolysis as well as oxidative phosphorylation (Fig. S5A-H), overall the ECAR/OCR ratio was higher for BCP-treated macrophages suggesting that it may be a more potent inducer of glycolysis [Fig. 2 (J)]. Furthermore, when ATP production rate was assessed post BCP treatment, total cellular ATP

was significantly enhanced at all time points tested, with BCP-treatment resulting in an increase in glycoATP production rates and a decrease in mitoATP production rates [Fig. 2 (D)]. Taken together, these data indicate that human macrophages promote glycolytic metabolism upon BCP stimulation.

Macrophage polarization and metabolic reprogramming by BCP crystals is dependent on particle uptake.

Having established that BCP crystals can induce a metabolic switch in human macrophages, it was of interest to determine if these responses are dependent on particle uptake. To test this, macrophages were pre-treated with the actin polymerization inhibitor, Latrunculin B (1 μM) (to inhibit phagocytosis) for 45 minutes prior to stimulation with BCP crystals. Results demonstrate that BCP induced CXCL9 and CXCL10 mRNA expression was significantly reduced in the presence of latrunculin B [Fig. 3 (A & B)]. Inhibiton of particle uptake also significantly reduced BCP crystal induced IL-8 production [Fig. 3 (C)] as well as mRNA expression of the glycolytic markers, HK2, Glut1 and HIF1α [Fig. 3 (D-F)]. To ensure that these observations were not due to loss of membrane integrity, which has been associated with Latrunculin B (37), cells were also pre-treated with the alternative actin polymerization inhibitors Cytochalasin D and B (5 μM) and the dynamin inhibitor, Dynasore (80 μM) prior to stimulation with BCP crystals. Similar trends were observed with all three inhibitors of phagocytosis (Fig. S7). Taken together, this indicates that particle uptake is essential for BCP crystal mediated activation of macrophages and glycolytic gene expression.

Inhibition of Glycolysis abrogates BCP crystal induced macrophage polarization and alarmin expression.

To elucidate if direct inhibition of glycolysis abrogates BCP crystal induced macrophage polarization, cells were stimulated with BCP crystals as described, in the presence or absence of the glycolytic inhibitor, 2-DG. Pre-treatment of cells with 2-DG resulted in a significant decrease of BCP induced CXCL9 and CXCL10 mRNA expression [Fig. 4 (A & B)]. We have previously demonstrated that BCP crystals strongly upregulate expression of the alarmin S100A8 (29, 30) which together with S100A9, is heavily implicated in driving catabolic processes in OA (38–40). mRNA expression of S100A8 was significantly inhibited in the presence of 2-DG [(Fig. 4 (C)] suggesting that inhibition of macrophage metabolic reprogramming impacts on the ability of BCP crystals to induce alarmin expression. Finally, inhibition of glycolysis with 2-DG decreased surface maker expression of CD40, CD80 and CD86 in BCP treated macrophages [Fig. 4 (D & E)]. Taken together, the results suggest that glycolytic blockade inhibits BCP-induced pro-inflammatory effects in macrophages.

Discussion

While several studies have demonstrated that impaired mitochondrial dysfunction contributes to pro-catabolic processes in OA chondrocytes, the factors contributing to this phenomenon have not been fully characterized (21). Furthermore, there have been few studies examining metabolic reprogramming in OA synovial fibroblasts or macrophages. During infection, stimulation of pattern recognition receptors (PRRs) leads to enhanced glycolysis which enables immune cells to generate sufficient ATP and pro-inflammatory mediators required to carry out effector functions (3). It is now well accepted that sterile tissue injury can provoke an immune response analogous to that seen during infection and that endogenous molecules generated upon tissue damage are capable of exerting similar effects on cellular processes. Hence, while the switch to a highly active metabolic state is necessary for immune cell activation during infection, metabolic reprogramming by DAMPs/alarmins in the absence of infection has the potential to exacerbate existing inflammation. We now demonstrate that BCP crystals which are OA-associated DAMPs, polarize primary human macrophages towards an M1-like phenotype, enhancing expression of M1-macrophage associated markers and elevating expression of surface maturation markers. Furthermore, BCP crystal stimulation promotes a bioenergetic switch favouring glycolysis and this is accompanied by increased expression of HIF1α, GLUT1 and hexokinase 2, all of which are surrogate markers of glycolysis. Finally, BCP-induced expression of M1 markers and the alarmin, S100A8, was inhibited in the presence of glycolytic inhibitor, 2DG, suggesting that BCP-induced macrophage polarization and inflammation may be dependent on metabolic reprogramming.

Particulates such as calcium oxalate crystals have previously been reported to promote M1 macrophage polarization (41) and, while a number of studies have investigated metabolic reprogramming in human immune cells in response to exogenous pathogen associated molecules (i.e. PAMPs), to our knowledge this is the first report of an endogenous particulate impacting on immune cell metabolism. We demonstrate that human macrophages stimulated with BCP crystals upregulate both glycolysis and oxidative phosphorylation within hours of activation however, the overall glycolytic and ATP production rate is higher. In our hands, LPS stimulation also resulted in enhanced glycolysis and oxidative phosphorylation in human macrophages however, BCP crystals promoted a higher ECAR:OCR ratio than LPS which is considered a potent PAMP. The observed effects of LPS on ECAR and OCR rates differs from reports in murine DC demonstrating that LPS strongly upregulates aerobic glycolysis whilst simultaneously downregulating oxidative phosphorylation via the action of iNOS-derived NO (42, 43). There is, however, controversy regarding the expression/activity of iNOS in human immune cells (44, 45) and our finding is in agreement with a recent study by Malinarich *et al*. who reported that, while mature human DC are more glycolytic than immature DC, they do not entirely downregulate oxidative phosphorylation, and instead display a more "balanced" switch to glycolysis whereby glycolysis and oxidative phosphorylation are both upregulated (46).

BCP crystals have previously been reported to upregulate the expression of inflammatory and catabolic mediators in a number of cell types implicated in OA (24, 47–49). Our results show that, in addition to cytokines, chemokines and MMPs, BCP crystals can also upregulate expression of the key glycolytic enzymes, hexokinase 2, GLUT1 and HIF1α, an effect which was attenuated in the presence of phagocytosis inhibitors. Furthermore, when glycolysis was inhibited with the glucose analog, 2-DG, we observed a notable decrease in

M1-macrophage marker expression, in addition to S100A8, which is a key OA-associated DAMP. Further analysis will determine if metabolic targeting impacts on downstream targets of S100A8 which include cytokines such as IL-6 and IL-8, as well as MMPs 1, 9 and 13 (29, 50). Interestingly, BCP crystals themselves were potent drivers of IL-8 expression in our hands. This may represent a feed forward mechanism whereby BCP-induced S100A8 drives expression of IL-8, albeit it should be noted that, while S100A8 is known to stimulate the synovial membrane to generate pro-inflammatory mediators, including IL-8 (51) in OA, this chemokine is generally not implicated in Milwaukee Shoulder Syndrome which is also characterized by BCP crystal deposition (25). Further study is required to fully elucidate the relationship between BCP crystals, IL-8 and the downstream effects of S100A8 production. It will also be necessary to determine whether BCP crystals drive metabolic reprogramming in synoviocytes from OA patient samples and whether glycolytic inhibitors impact on inflammatory/catabolic processes. Indeed, upregulation of glucose transport and an increase in glycolytic metabolism has been demonstrated in OA and particularly in chondrocytes were accumulation of lactic acid contributes to matrix acidification and impaired ECM synthetic function (52–55). Less is known regarding metabolic disturbances in OA-synoviocytes, however an increase in the glycolysis/OXPHOS ratio has been observed in OA-FLS (21). Furthermore, silencing of PHD2, a global negative regulator of HIF-1α expression decreased expression of angiogenic genes, while high glucose levels were shown to induce ROS and VEGF in OA-FLS further implicating a metabolic switch and increased glucose transport in synovial joint cells in OA (56, 57).

While the field of immunometabolism is still in its infancy and much remains to be learned regarding the impact of metabolic reprogramming on disease pathogenesis, ultimately it may be possible to modulate metabolic changes in polarized macrophages by

specifically targeting key glycolytic enzymes. However, extreme caution is required given the strong potential for off target effects. This is of particular importance in OA given that chondrocytes, in particular, exist in a hypoxic environment and rely on HIF1α and glycolysis to maintain homeostasis. Currently, there are no drugs available to target BCP crystal deposition in the OA joint and subsequent inflammatory responses, however, based on the above findings, we propose that targeting BCP-and DAMP-induced metabolic reprogramming represents a novel avenue that requires further consideration and exploration.

Acknowledgements: We would like to thank Dr Eoin O'Brien and Eva Desmond for technical assistance.

Author Contributions: OM and AD contributed to conception and design of the study, analysis and interpretation of the data, drafting of the article. DK and GM contributed to the interpretation of data and provision of study materials.

Funding source: This study was supported by a Trinity College Dublin Postgraduate Research Studentship.

Competing interest statement: The authors declare no conflicts of interest.

References

1. Loeser, R. F., J. A. Collins, and B. O. Diekman. 2016. Ageing and the pathogenesis of osteoarthritis. *Nat Rev Rheumatol* 12: 412–420.

2. Mobasheri, A. 2013. The Future of Osteoarthritis Therapeutics: Targeted Pharmacological Therapy. *Curr. Rheumatol. Rep.* 15: 364.

3. O'Neill, L. A. J., R. J. Kishton, and J. Rathmell. 2016. A guide to immunometabolism for immunologists. *Nat Rev Immunol* 16: 553–565.

4. Pearce, E. L., and E. J. Pearce. 2013. Metabolic pathways in immune cell activation and quiescence. *Immunity* 38: 633–643.

5. Pearce, E. L., M. C. Poffenberger, C.-H. Chang, and R. G. Jones. 2013. Fueling immunity: insights into metabolism and lymphocyte function. *Science* 342: 1242454.

6. Loftus, R. M., and D. K. Finlay. 2016. Immunometabolism: Cellular Metabolism Turns Immune Regulator. *J. Biol. Chem.* 291: 1–10.

7. San-Millán, I., and G. A. Brooks. 2017. Reexamining cancer metabolism: Lactate production for carcinogenesis could be the purpose and explanation of the Warburg Effect. *Carcinogenesis* 38: 119–133.

8. Palsson-McDermott, E. M., and L. A. J. O'Neill. 2013. The Warburg effect then and now: From cancer to inflammatory diseases. *BioEssays* 35: 965–973.

9. Dang, E. V, J. Barbi, H.-Y. Yang, D. Jinasena, H. Yu, Y. Zheng, Z. Bordman, J. Fu, Y. Kim, H.-R. Yen, W. Luo, K. Zeller, L. Shimoda, S. L. Topalian, G. L. Semenza, C. V Dang, D. M. Pardoll, and F. Pan. 2011. Control of T(H)17/T(reg) balance by hypoxia-inducible factor 1. *Cell* 146: 772–

784.

10. Russell, D. G., L. Huang, and B. C. VanderVen. 2019. Immunometabolism at the interface between macrophages and pathogens. *Nat. Rev. Immunol.* .

11. Diskin, C., and E. M. Pålsson-McDermott. 2018. Metabolic Modulation in Macrophage Effector Function. *Front. Immunol.* 9: 270.

12. Osborn, O., and J. M. Olefsky. 2012. The cellular and signaling networks linking the immune system and metabolism in disease. *Nat Med* 18: 363–374.

13. Yin, Y., S.-C. Choi, Z. Xu, D. J. Perry, H. Seay, B. P. Croker, E. S. Sobel, T. M. Brusko, and L. Morel. 2015. Normalization of CD4+ T cell metabolism reverses lupus. *Sci. Transl. Med.* 7: 274ra18 LP-274ra18.

14. Lee, C.-F., Y.-C. Lo, C.-H. Cheng, G. J. Furtmüller, B. Oh, V. Andrade-Oliveira, A. G. Thomas, C. E. Bowman, B. S. Slusher, M. J. Wolfgang, G. Brandacher, and J. D. Powell. 2017. Preventing Allograft Rejection by Targeting Immune Metabolism. *Cell Rep.* 13: 760–770.

15. Bettencourt, I. A., and J. D. Powell. 2017. Targeting Metabolism as a Novel Therapeutic Approach to Autoimmunity, Inflammation, and Transplantation. *J. Immunol.* 198: 999 LP-1005.

16. Biniecka, M., M. Canavan, T. McGarry, W. Gao, J. McCormick, S. Cregan, L. Gallagher, T. Smith, J. J. Phelan, J. Ryan, J. O'Sullivan, C. T. Ng, D. J. Veale, and U. Fearon. 2016. Dysregulated bioenergetics: a key regulator of joint inflammation. *Ann. Rheum. Dis.* 75: 2192 LP-2200.

17. McGarry, T., M. Biniecka, W. Gao, D. Cluxton, M. Canavan, S. Wade, S. Wade, L. Gallagher, C. Orr, D. J. Veale, and U. Fearon. 2017. Resolution of TLR2-induced inflammation

through manipulation of metabolic pathways in Rheumatoid Arthritis. *Sci. Rep.* 7: 43165.

18. June, R. K., R. Liu-Bryan, F. Long, and T. M. Griffin. 2016. Emerging role of metabolic signaling in synovial joint remodeling and osteoarthritis. *J. Orthop. Res.* 34: 2048–2058.

19. Liu-Bryan, R. 2015. Inflammation and intracellular metabolism: new targets in OA. *Osteoarthr. Cartil.* 23: 1835–1842.

20. Kluzek, S., J. L. Newton, and N. K. Arden. 2015. Is osteoarthritis a metabolic disorder? *Br. Med. Bull.* 115: 111–121.

21. Mobasheri, A., M. P. Rayman, O. Gualillo, J. Sellam, P. van der Kraan, and U. Fearon. 2017. The role of metabolism in the pathogenesis of osteoarthritis. *Nat Rev Rheumatol* 13: 302–311.

22. Grishko, V. I., R. Ho, G. L. Wilson, and A. W. Pearsall. 2009. Diminished mitochondrial DNA integrity and repair capacity in OA chondrocytes. *Osteoarthritis Cartilage* 17: 107–113.

23. Gobelet, C., and J. C. Gerster. 1984. Synovial fluid lactate levels in septic and non-septic arthritides. *Ann. Rheum. Dis.* 43: 742–745.

24. Bulysheva, A. A., N. Sori, and M. P. Francis. 2018. Direct crystal formation from micronized bone and lactic acid: The writing on the wall for calcium-containing crystal pathogenesis in osteoarthritis? *PLoS One* 13: e0202373–e0202373.

25. McCarthy, G. M., and A. Dunne. 2018. Calcium crystal deposition diseases — beyond gout. *Nat. Rev. Rheumatol.* 14: 592–602.

26. Stack, J., and G. McCarthy. 2016. Basic calcium phosphate crystals and osteoarthritis pathogenesis: novel pathways and potential targets. *Curr Opin Rheumatol* 28: 122–126.

27. Nadra, I., J. C. Mason, P. Philippidis, O. Florey, C. D. W. Smythe, G. M. McCarthy, R. C. Landis, and D. O. Haskard. 2005. Proinflammatory Activation of Macrophages by Basic Calcium Phosphate Crystals via Protein Kinase C and MAP Kinase Pathways. *Circ. Res.* 96: 1248 LP-1256.

28. Nasi, S., A. So, C. Combes, M. Daudon, and N. Busso. 2016. Interleukin-6 and chondrocyte mineralisation act in tandem to promote experimental osteoarthritis. *Ann. Rheum. Dis.* 75: 1372 LP-1379.

29. Corr, E. M., C. C. Cunningham, L. Helbert, G. M. McCarthy, and A. Dunne. 2017. Osteoarthritis-associated basic calcium phosphate crystals activate membrane proximal kinases in human innate immune cells. *Arthritis Res. Ther.* 19.

30. Cunningham, C. C., E. Mills, L. A. Mielke, L. K. O'Farrell, E. Lavelle, A. Mori, G. M. McCarthy, K. H. G. Mills, and A. Dunne. 2012. Osteoarthritis-associated basic calcium phosphate crystals induce pro-inflammatory cytokines and damage-associated molecules via activation of Syk and PI3 kinase. *Clin. Immunol.* 144.

31. Cunningham, C. C., E. M. Corr, G. M. McCarthy, and A. Dunne. 2016. Intra-articular basic calcium phosphate and monosodium urate crystals inhibit anti-osteoclastogenic cytokine signalling. *Osteoarthr. Cartil.* 24.

32. Pazár, B., H.-K. Ea, S. Narayan, L. Kolly, N. Bagnoud, V. Chobaz, T. Roger, F. Lioté, A. So, and N. Busso. 2011. Basic Calcium Phosphate Crystals Induce Monocyte/Macrophage IL-1β Secretion through the NLRP3 Inflammasome In Vitro. *J. Immunol.* 186: 2495–2502.

33. Corr, E. M., C. C. Cunningham, L. Helbert, G. M. McCarthy, and A. Dunne. 2017. Osteoarthritis-associated basic calcium phosphate crystals activate membrane proximal

kinases in human innate immune cells. *Arthritis Res. Ther.* 19: 23.

34. Nasi, S., H.-K. Ea, F. Lioté, A. So, and N. Busso. 2016. Sodium Thiosulfate Prevents Chondrocyte Mineralization and Reduces the Severity of Murine Osteoarthritis. *PLoS One* 11: e0158196.

35. Schulz, D., Y. Severin, V. R. T. Zanotelli, and B. Bodenmiller. 2019. In-Depth Characterization of Monocyte-Derived Macrophages using a Mass Cytometry-Based Phagocytosis Assay. *Sci. Rep.* 9: 1925.

36. Van den Bossche, J., L. A. O'Neill, and D. Menon. 2017. Macrophage Immunometabolism: Where Are We (Going)? *Trends Immunol.* 38: 395–406.

37. Pergola, C., K. Schubert, S. Pace, J. Ziereisen, F. Nikels, O. Scherer, S. Hüttel, S. Zahler, A. M. Vollmar, C. Weinigel, S. Rummler, R. Müller, M. Raasch, A. Mosig, A. Koeberle, and O. Werz. 2017. Modulation of actin dynamics as potential macrophage subtype-targeting anti-tumour strategy. *Sci. Rep.* 7: 1–12.

38. Zreiqat, H., D. Belluoccio, M. M. Smith, R. Wilson, L. A. Rowley, K. Jones, Y. Ramaswamy, T. Vogl, J. Roth, J. F. Bateman, and C. B. Little. 2010. S100A8 and S100A9 in experimental osteoarthritis. *Arthritis Res. Ther.* 12: R16.

39. Van Lent, P. L. E. M., A. B. Blom, R. F. P. Schelbergen, A. Slöetjes, F. P. J. G. Lafeber, W. F. Lems, H. Cats, T. Vogl, J. Roth, and W. B. Van Den Berg. 2012. Active involvement of alarmins S100A8 and S100A9 in the regulation of synovial activation and joint destruction during mouse and human osteoarthritis. *Arthritis Rheum.* 64: 1466–1476.

40. P., S. R. F., B. A. B., van den B. M. H. J., S. Annet, A. Shahla, S. B. Wim, M. J. S., V. Thomas, R. Johannes, van den B. W. B., and van L. P. L. E. M. 2011. Alarmins S100A8 and

S100A9 elicit a catabolic effect in human osteoarthritic chondrocytes that is dependent on Toll-like receptor 4. *Arthritis Rheum.* 64: 1477–1487.

41. Dominguez-Gutierrez, P. R., S. Kusmartsev, B. K. Canales, and S. R. Khan. 2018. Calcium Oxalate Differentiates Human Monocytes Into Inflammatory M1 Macrophages. *Front. Immunol.* 9: 1863.

42. Kelly, B., and L. A. J. O'Neill. 2015. Metabolic reprogramming in macrophages and dendritic cells in innate immunity. *Cell Res.* 25: 771–784.

43. Everts, B., E. Amiel, S. C. C. Huang, A. M. Smith, C. H. Chang, W. Y. Lam, V. Redmann, T. C. Freitas, J. Blagih, G. J. W. Van Der Windt, M. N. Artyomov, R. G. Jones, E. L. Pearce, and E. J. Pearce. 2014. TLR-driven early glycolytic reprogramming via the kinases TBK1-IKKε supports the anabolic demands of dendritic cell activation. *Nat. Immunol.* 15: 323–332.

44. Thomas, A. C., and J. T. Mattila. 2014. "Of mice and men": Arginine metabolism in macrophages. *Front. Immunol.* 5: 1–7.

45. Everts, B., E. Amiel, G. J. W. Van Der Windt, T. C. Freitas, R. Chott, K. E. Yarasheski, E. L. Pearce, and E. J. Pearce. 2012. Commitment to glycolysis sustains survival of NO-producing inflammatory dendritic cells. *Blood* 120: 1422–1431.

46. Malinarich, F., K. Duan, R. A. Hamid, A. Bijin, W. X. Lin, M. Poidinger, A.-M. Fairhurst, and J. E. Connolly. 2015. High Mitochondrial Respiration and Glycolytic Capacity Represent a Metabolic Phenotype of Human Tolerogenic Dendritic Cells. *J. Immunol.* 194: 5174–5186.

47. McCarthy, G. M., P. R. Westfall, I. Masuda, P. A. Christopherson, H. S. Cheung, and P. G. Mitchell. 2001. Basic calcium phosphate crystals activate human osteoarthritic synovial fibroblasts and induce matrix metalloproteinase-13 (collagenase-3) in adult porcine articular

chondrocytes. *Ann. Rheum. Dis.* 60: 399 LP-406.

48. Bai, G., D. S. Howell, G. A. Howard, B. A. Roos, and H. S. Cheung. 2001. Basic calcium phosphate crystals up-regulate metalloproteinases but down-regulate tissue inhibitor of metalloproteinase-1 and -2 in human fibroblasts. *Osteoarthr. Cartil.* 9: 416–422.

49. Morgan, M. P., L. C. Whelan, J. D. Sallis, C. J. McCarthy, D. J. Fitzgerald, and G. M. McCarthy. 2004. Basic calcium phosphate crystal–induced prostaglandin E2 production in human fibroblasts: Role of cyclooxygenase 1, cyclooxygenase 2, and interleukin-1β. *Arthritis Rheum.* 50: 1642–1649.

50. Cunningham, C. C., E. Mills, L. A. Mielke, L. K. O'Farrell, E. Lavelle, A. Mori, G. M. McCarthy, K. H. G. Mills, and A. Dunne. 2012. Osteoarthritis-associated basic calcium phosphate crystals induce pro-inflammatory cytokines and damage-associated molecules via activation of Syk and PI3 kinase. *Clin. Immunol.* 144: 228–36.

51. Wang, S., R. Song, Z. Wang, Z. Jing, S. Wang, and J. Ma. 2018. S100A8/A9 in Inflammation . *Front. Immunol.* 9: 1298.

52. Johnson, K., A. Jung, A. Murphy, A. Andreyev, J. Dykens, and R. Terkeltaub. 2000. Mitochondrial oxidative phosphorylation is a downstream regulator of nitric oxide effects on chondrocyte matrix synthesis and mineralization. *Arthritis Rheum.* 43: 1560–1570.

53. Wang, Y., X. Zhao, M. Lotz, R. Terkeltaub, and R. Liu-Bryan. 2015. Mitochondrial Biogenesis Is Impaired in Osteoarthritis Chondrocytes but Reversible via Peroxisome Proliferator–Activated Receptor γ Coactivator 1α. *Arthritis Rheumatol.* 67: 2141–2153.

54. Maneiro, E., M. A. Martín, M. C. de Andres, M. J. López-Armada, J. L. Fernández-Sueiro, P. del Hoyo, F. Galdo, J. Arenas, and F. J. Blanco. 2003. Mitochondrial respiratory activity is

altered in osteoarthritic human articular chondrocytes. *Arthritis Rheum.* 48: 700–708.

55. Blanco, F. J., M. J. López-Armada, and E. Maneiro. 2004. Mitochondrial dysfunction in osteoarthritis. *Mitochondrion* 4: 715–728.

56. Muz, B., H. Larsen, L. Madden, S. Kiriakidis, and E. M. Paleolog. 2012. Prolyl hydroxylase domain enzyme 2 is the major player in regulating hypoxic responses in rheumatoid arthritis. *Arthritis Rheum.* 64: 2856–2867.

57. Tsai, C.-H., Y.-C. Chiang, H.-T. Chen, P.-H. Huang, H.-C. Hsu, and C.-H. Tang. 2013. High glucose induces vascular endothelial growth factor production in human synovial fibroblasts through reactive oxygen species generation. *Biochim. Biophys. Acta - Gen. Subj.* 1830: 2649–2658.

Figures

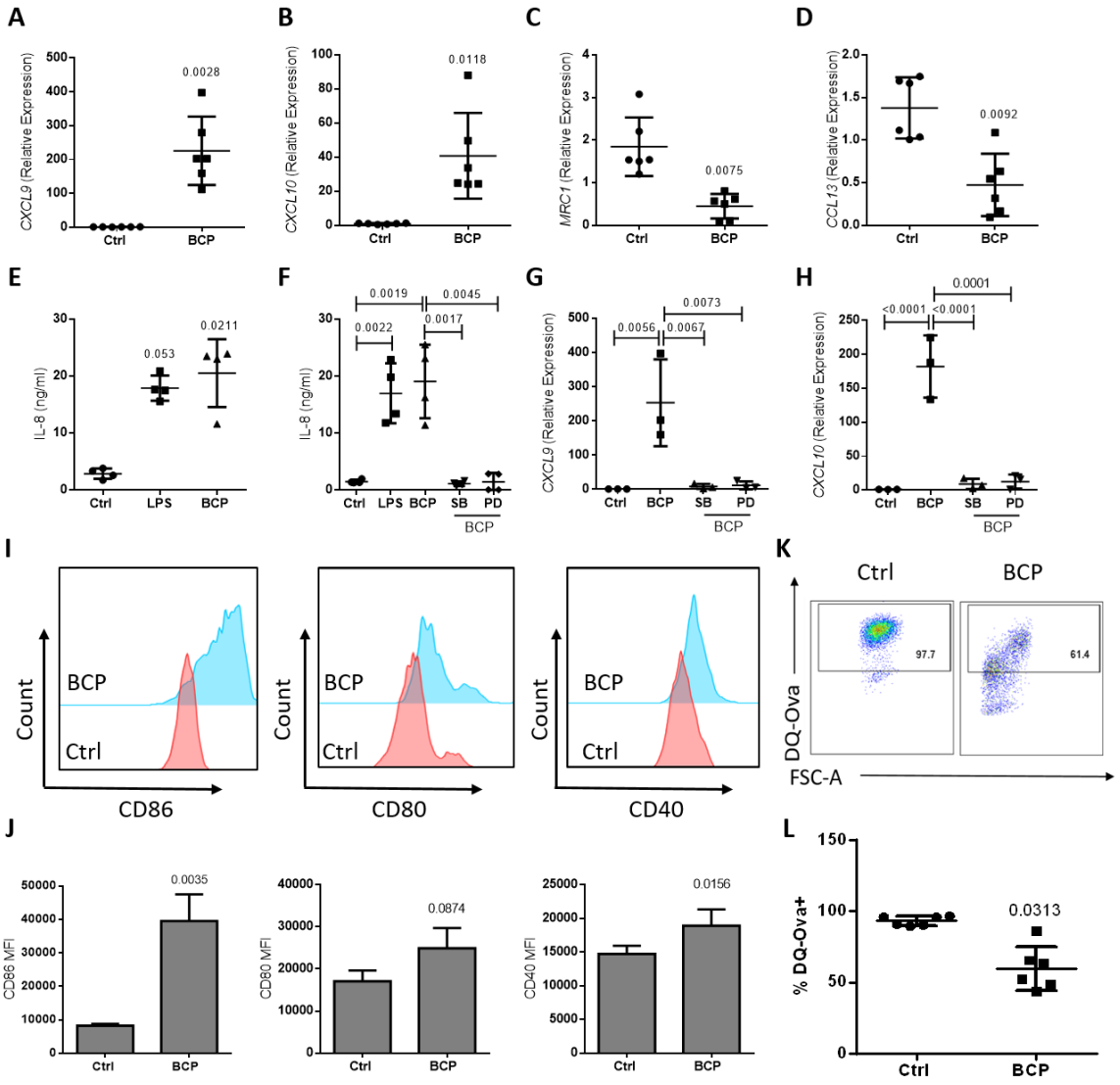

Figure 1: BCP crystals promote M1 macrophage polarization. Primary human macrophages (1 x 10^6) were stimulated with BCP (50 µg/ml) for 24 hours. (A-D) mRNA expression of CXCL9, CXCL10, MRC1 and CCL13 was analysed by real-time PCR (N=6, n=3). (E) IL-8 cytokine production in cell supernatants was analysed by ELISA (N=4, n=3). (F-H) Macrophages were pre-treated with the p38 and ERK MAP kinase inhibitors (SB203580; 20 µM, PD98059; 20 µM) for 45 min prior to stimulation with BCP (50 µg/ml) for 24 hours. IL-8 cytokine production in cell supernatants was analysed by ELISA (N=4, n=3) and mRNA levels of CXCL9 and CXCL10

were analyzed by real-time PCR (N=6, n=3). (I) Representative histograms from one experiment of the macrophage maturation markers CD86, CD80 and CD40 were determined by flow cytometry and (J) Pooled data (N=5, n=2) depicts mean Fluorescence Intensity (MFI) of surface marker expression. Macrophages were stimulated with BCP (50 μg/ml) for 24 hours and then incubated with FITC-conjugated DQ-ovalbumin (DQ-Ova; 500 ng/ml) for 20 min prior to analysis by flow cytometry. (K) Representative dot plots depicting DQ-Ova uptake by BCP treated macrophages. (L) Pooled data (N=5, n=2) depicts percentage DQ-Ova uptake. All data is represented as Mean ± SEM. Data was analysed using Kruskal Wallis with Dunn's post-test for cytokine assays and one-way ANOVA with Tukey post-test for real-time PCR assays. Data was analysed using Wilcoxon Signed Rank test for Flow Cytometry assays.

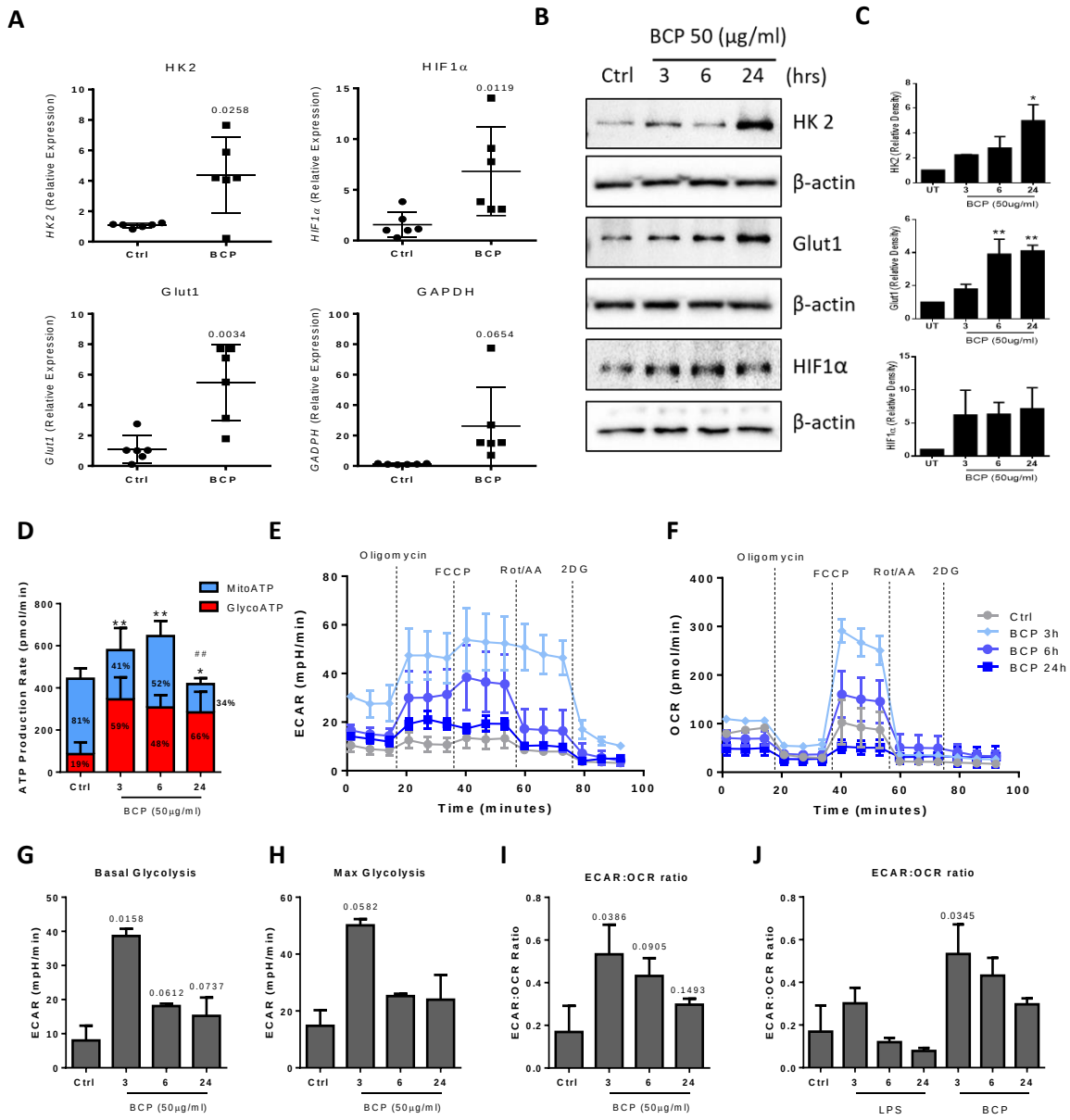

Figure 2: BCP crystals alter macrophage metabolism and promote glycolysis. Primary human macrophages (1 x 10^6) were stimulated with BCP (50 μg/ml) for 24 hours. (A) mRNA expression of glycolytic markers GLUT1, HK2, HIF1α and GAPDH were analysed by real-time PCR (N=6, n=3). (B) Representative western blots demonstrating expression of HK2 and Glut 1 in whole cell lysates in response to BCP crystals over time. (C) Densitometric analysis of immunoblots (N=3) using ImageJ software. Bar graphs illustrate the Mean ± SEM increase in protein expression relative to untreated control and normalised to β-actin housekeeping

protein. (D & E) Representative glycolysis (ECAR) and oxidative phosphorylation (OCR) Seahorse bioenergetics profiles before and after injections of oligomycin (1 µM), FCCP (1 µM), antimycin A (500 nM)/Rotenone (500 nM), and 2-DG (25mM) post stimulation with BCP crystals (50 µg/ml). Bar graphs demonstrating (F) ATP production rate (G) basal glycolysis, (H) max glycolysis and (I) the ratio of glycolysis: oxidative phosphorylation (ECAR:OCR) in response to BCP crystal stimulation or (J) ECAR:OCR ratio in LPS or BCP treated cells. (N=3, n=4). All data is represented as Mean ± SEM. Data was analysed using was analysed using a paired Student's t test for real-time PCR assays, a one-way ANOVA for densitometric analysis of immunoblots. Data was analysed using Kruskal Wallis with Dunn's post-test was used for all Seahorse calculations.

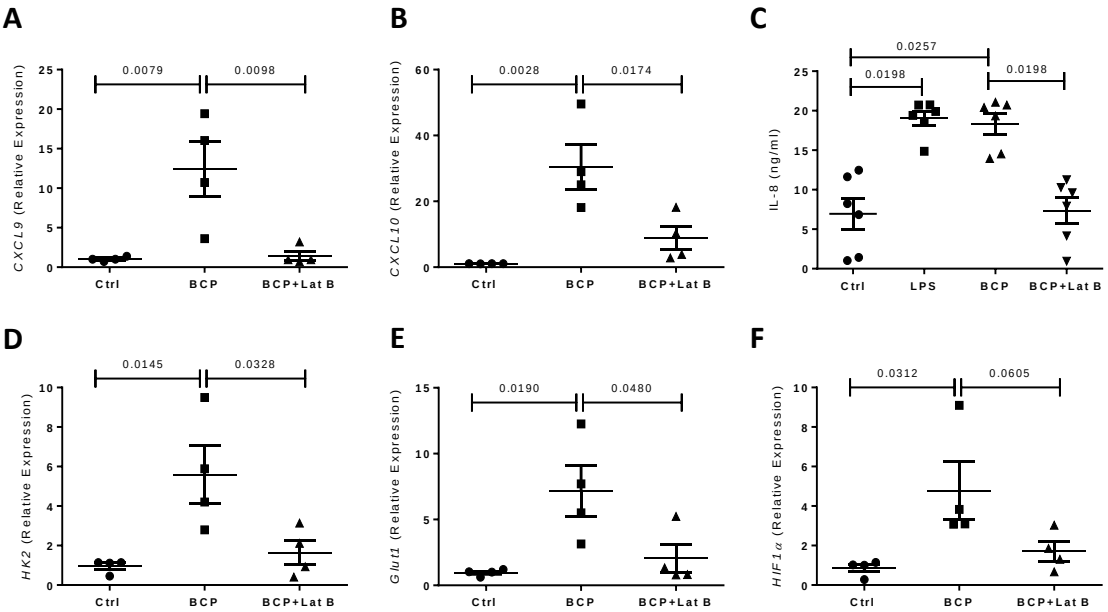

Figure 3: Macrophage polarization and metabolic reprogramming by BCP crystals is dependent on particle uptake. Primary human macrophages (1 x 10^6) were treated with BCP (50 µg/ml) alone or were pre-treated with the actin polymerization inhibitor, Latrunculin B (1 µM), prior to treatment with BCP (50 µg/ml). (A & B) Graphs demonstrating mRNA levels of

CXCL9 and CXCL10 (N=4, n=3). (C) Cytokine levels of IL-8 in cell supernatants ((N=6, n=3). (D-F) mRNA expression of the glycolytic markers HK2, Glut1 and HIF1α (N=4, n=3). Alternatively primary human macrophages (1 x 10^6) were treated with BCP (50 µg/ml) alone or were pre-treated with the actin polymerization inhibitors, Cytochalsin D (5 µM), Cytochalsin B (5 µM) or the Dynamin inhibitor, Dynasore (80 µM) prior to treatment with BCP (50 µg/ml). (G & H) Graphs demonstrating mRNA levels of CXCL9 and CXCL10 (N=3, n=3). (I-K) mRNA expression of the glycolytic markers HK2, Glut1 and HIF1α (N=3, n=3). Data is represented as Mean ± SEM and analysed using Kruskal Wallis with Dunn's post-test for cytokine assays and one-way ANOVA with Tukey post-test for real-time PCR assays.

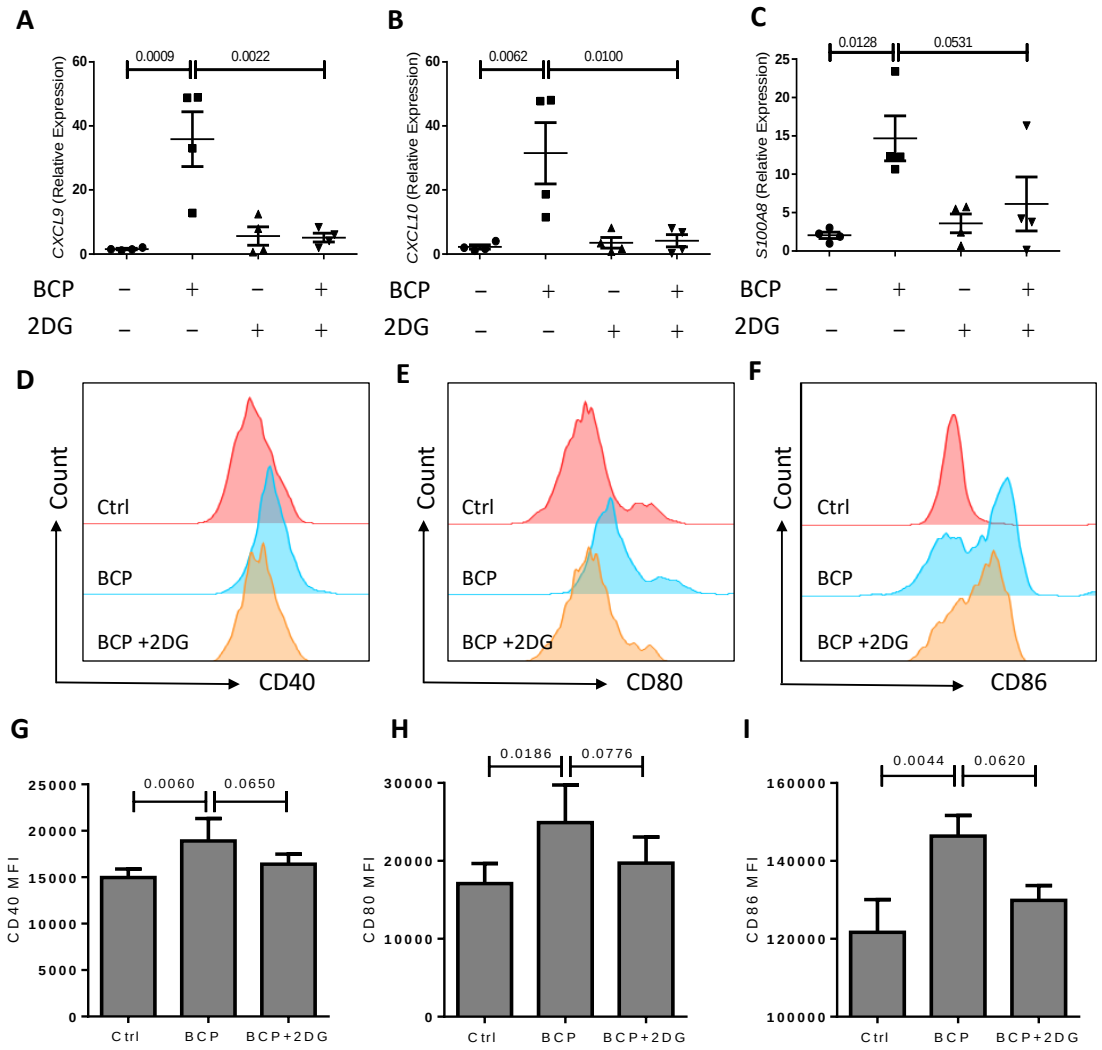

Figure 4: BCP crystal-induced macrophage polarization is reduced in the presence of the glycolytic inhibitor 2-DG. Primary human macrophages (1 x 10^6) were stimulated with BCP (50 µg/ml) in the presence or absence of 2-DG (25 mM) for 24 hours. (A-C) Graphs demonstrating mRNA levels of CXCL9, CXCL10 and S100A8 (N=4, n=3). (D) Representative histograms from one experiment demonstrating CD40, CD80 and CD86 surface marker expression. (E) Pooled data (N=4, n=2) depicts mean Fluorescence Intensity (MFI) of surface marker expression. Data is represented as Mean ± SEM Data and was analyzed using one-way ANOVA with Tukey post-test for real-time PCR assays and Kruskal Wallis for Flow cytometry assays.

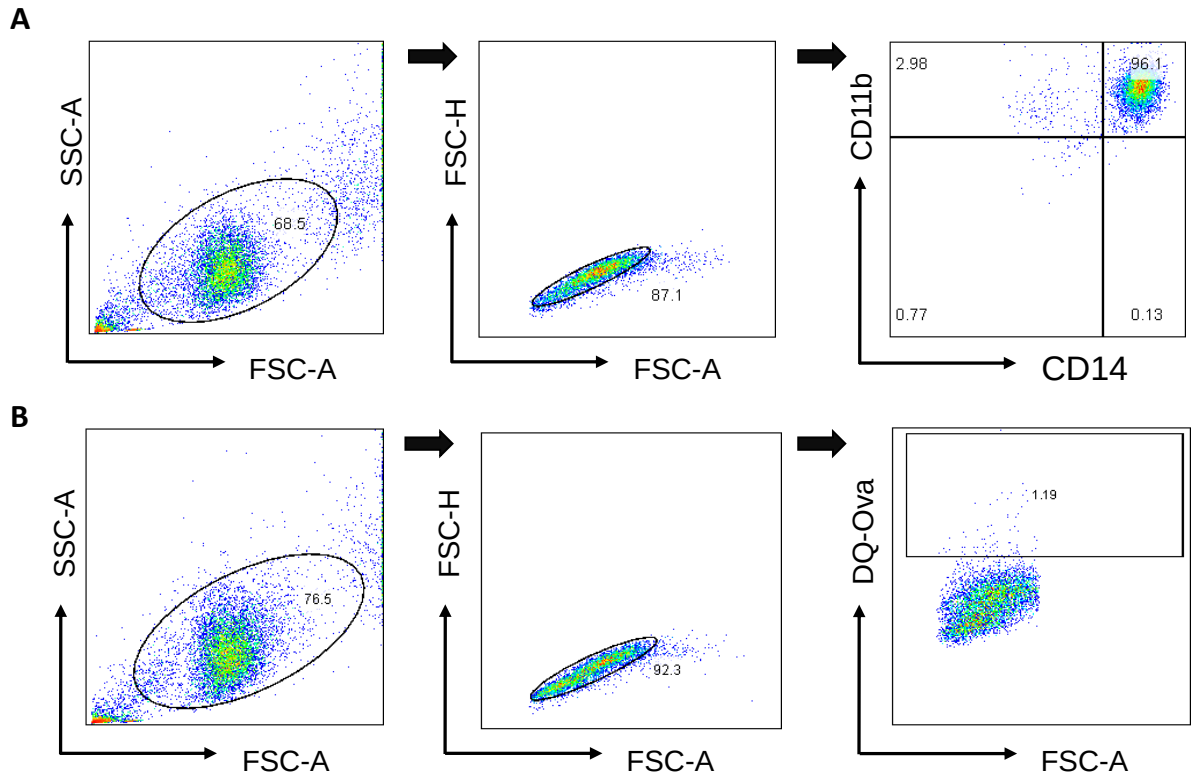

Supplementary Figure 1: Flow cytometry gating strategy. (A) To assess expression of the maturation markers CD40, CD80 and CD86 by macrophages, the macrophage population was first selected by FSC and SSC. Single cells were then gated on by FSC area and height. Viable cells were then selected on the basis of viability dye exclusion. Fully differentiated

macrophages were selected for by co-expression of CD14 and CD11b. (B) To measure DQ - Ova uptake, the macrophage population was first selected on the basis of FSC and SSC in order to exclude debris and dying cells. Single cells were then selected based on FSC area and height. The DQ-Ova+ cell gate was then drawn using control cells which were not incubated with DQ-Ova.

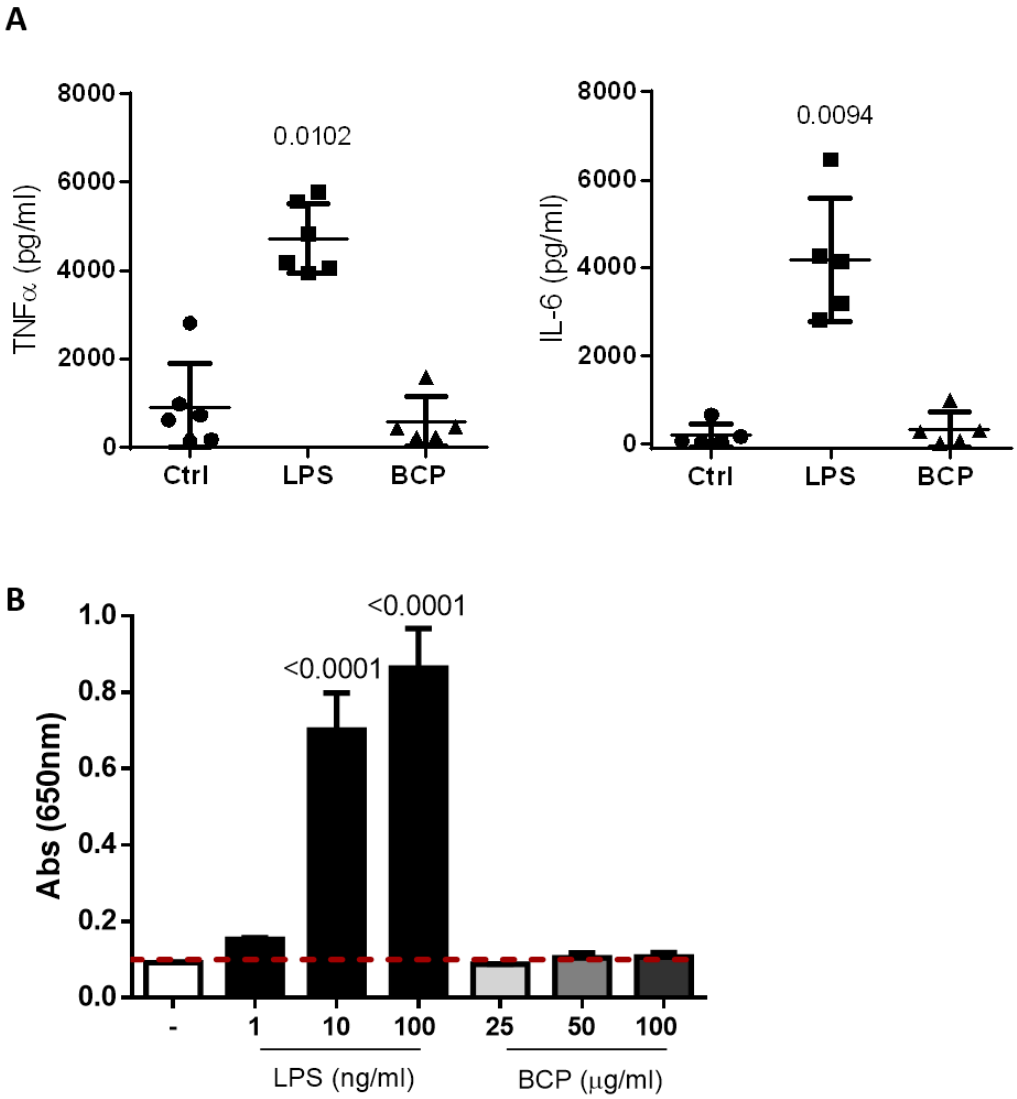

Supplementary Figure 2: BCP crystals are not contaminated with endotoxin and do not drive TNFα or IL-6. (A) Primary human macrophages (1 x 10^6) were treated with BCP crystals (50ug/ml) or LPS (100 ng/ml) as a positive control for 24 hours and cytokine levels of TNFα and IL-6 in cell supernatants were measured by ELISA. (B) BCP crystal preparations were

shown to be endotoxin free, using the HEK-Blue^{TM} hTLR4 assay system (Invivogen). The expression of SEAP, as measured by absorbance at 650nm, by BCP treated macrophages was comparable to untreated control cells. As a positive control, cells were treated with LPS (1 ng/ml, 10 ng/ml or 100 ng/ml). Data was analyzed using Kruskal Wallis with Dunns post-test and is represented as Mean ± SEM of 6 independent experiments (N=6, n=3).

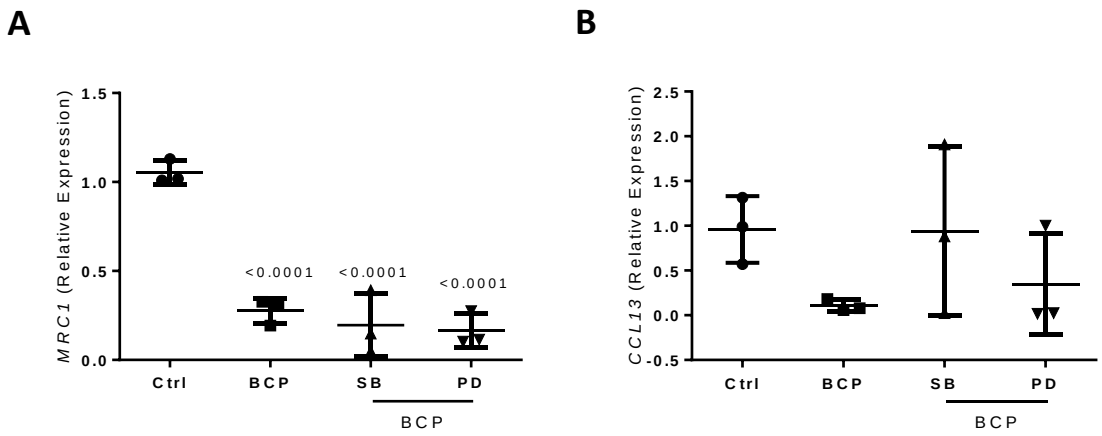

Supplementary Figure 3: Inhibition of MAP kinases does not effect BCP crystals induced responses on M2 macrophage markers. Macrophages were pre-treated with the p38 and ERK MAP kinase inhibitors (SB203580; 20 µM, PD98059; 20 µM) for 45 min prior to stimulation with BCP (50 µg/ml) for 24 hours. mRNA levels of MRC1 and CCL13 were analyzed by real-time PCR (N=3, n=3). Data is represented as Mean ± SEM and was analyzed using paired Student's t test.

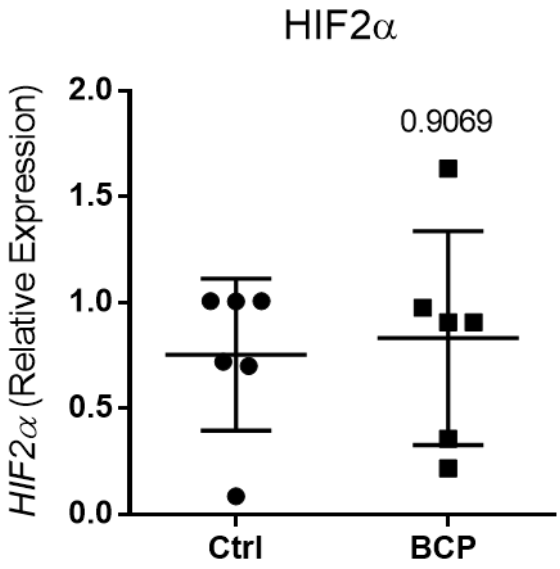

Supplementary Figure 4: BCP crystals do not affect expression of HIF2α. Primary human macrophages (1 x 10^6) were stimulated with BCP crystals (50 μg/ml) for 24 hours and mRNA expression of HIF2α was analysed by real-time PCR. Data was analyzed using Student's t test and is represented as Mean ± SEM of 6 independent experiments (N=6, n=3).

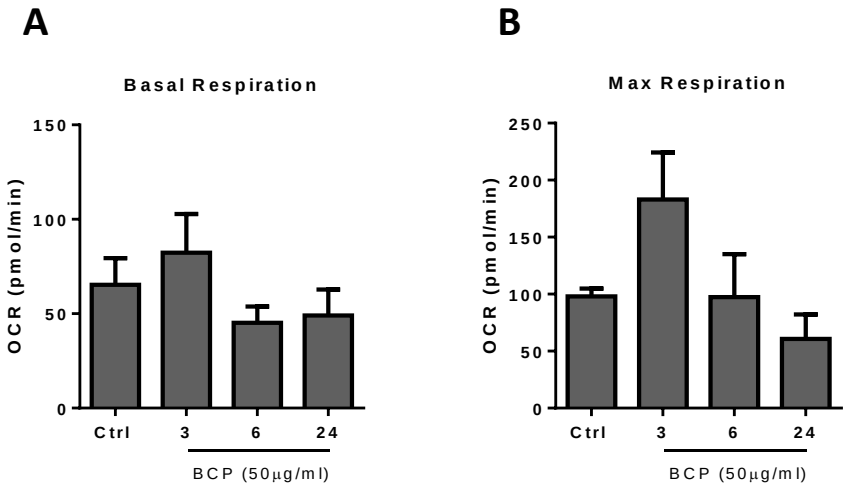

Supplementary Figure 5: Effect of BCP crystals on macrophage oxidative phosphorylation. Primary human macrophages (1 x 10^6) were stimulated with BCP (50 μg/ml) for 3, 6 or 24

hours. Bar graphs demonstrating basal respiration and max respiration in response to BCP crystal stimulation (N=3, n=4). Data is represented as Mean ± SEM and was analyzed by Kruskal Wallis.

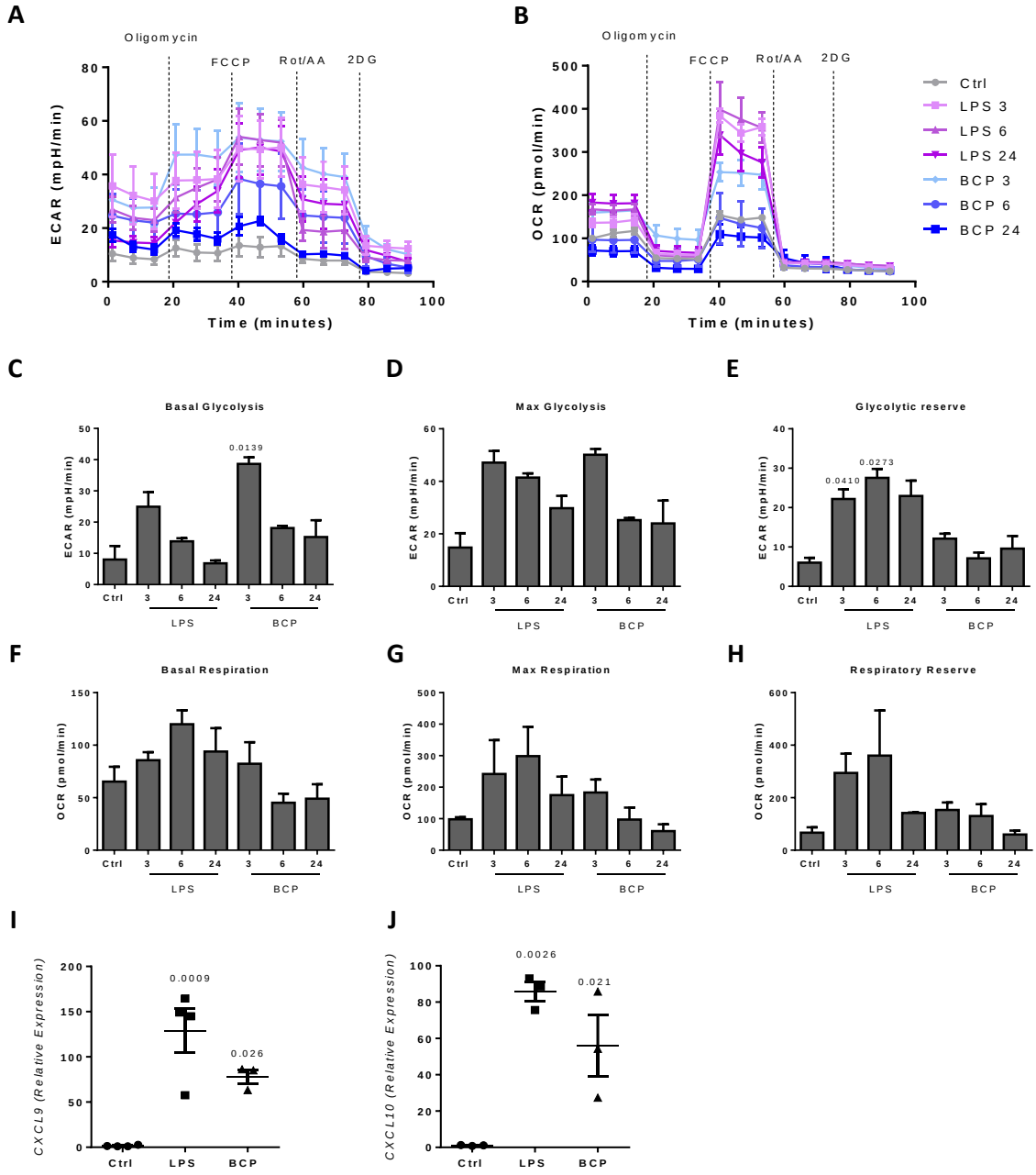

Supplementary Figure 6: Comparison of metabolic function and macrophage phenotype after LPS and BCP treatment. Primary human macrophages (1 x 10^6) were stimulated with BCP (50 µg/ml) for 3,6 or 24 hours. (A & B) Representative glycolysis (ECAR) and oxidative

phosphorylation (OCR) Seahorse bioenergetics profiles before and after injections of oligomycin (1 µM), FCCP (1 µM), antimycin A (500 nM)/Rotenone (500 nM), and 2-DG (25mM) post stimulation with BCP crystals (50 µg/ml) or LPS (100 ng/ml). Bar graphs demonstrating (C) basal glycolysis, (D) max glycolysis, (E) Glycolytic reserve, (F) Basal respiration, (G) Max respiration and (H) Respiratory reserve in response to LPS or BCP stimulation (N=3, n=4). (I & J) mRNA expression of CXCL9 and CXCL10 was analysed by real-time PCR (N=3, n=3). Data is represented as Mean ± SEM and was analyzed using Kruskal Wallis for Seahorse data and paired one-way ANOVA for real-time PCR assays.

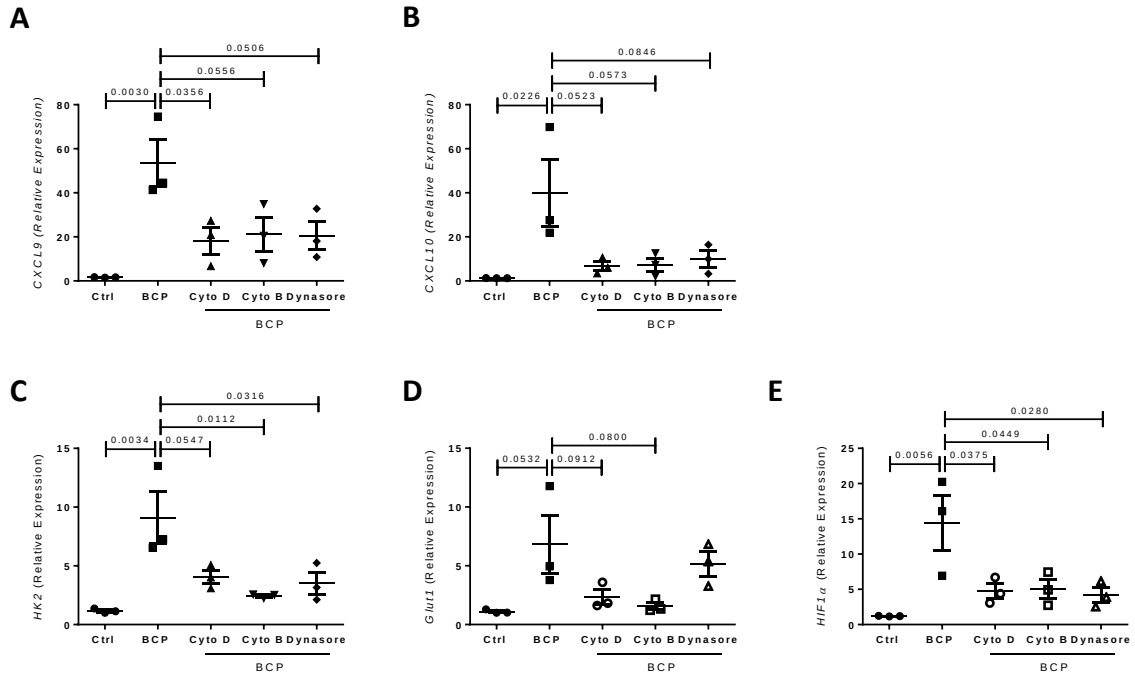

Supplementary Figure 7: Macrophage polarization and metabolic reprogramming by BCP crystals is dependent on particle uptake. Primary human macrophages (1 x 10^6) were treated with BCP (50 µg/ml) alone or were pre-treated were pre-treated with the actin polymerization inhibitors, Cytochalsin D (5 µM), Cytochalsin B (5 µM) or the Dynamin inhibitor, Dynasore (80 µM) prior to treatment with BCP (50 µg/ml). (A & B) Graphs demonstrating mRNA levels of CXCL9 and CXCL10 (N=3, n=3). (C-E) mRNA expression of the glycolytic markers HK2, Glut1

and HIF1α (N=3, n=3). Data is represented as Mean $\pm$ SEM and analysed using Kruskal Wallis with Dunn's post-test for cytokine assays and one-way ANOVA with Tukey post-test for real-time PCR assays.

Supplementary Methods

Reagents

Ultrapure lipopolysaccharide (LPS), p38 inhibitor (SB203580) and MEK/ERK inhibitor (PD98059) inhibitors were from Invivogen (Toulouse, France). BCP crystals in the form of Hydroxyapatite (HA) were synthesized by alkaline hydrolysis of brushite as described (33). Recombinant human M-CSF was from PeproTech (Rocky Hill,NJ). Lymphoprep was from Stemcell Technologies (Grenoble,France). Hexokinase 2 primary antibody was obtained from Novus Biologics, Glut1 primary antibody was obtained from abcam. 2-DG, Latrunculin B, Oligomycin, Antimycin A, Rotenone, FCCP, secondary antibodies, cell culture reagents and all other chemicals were from Sigma Aldrich (St. Louis, MO). Taqman probes were from applied biosystems. Primers for the Glycolytic genes (HK2, Glut1 and PFKB3) were from MicroSynth and primers for HIF1α, HIF2α and GAPDH were from Sigma Aldrich (St.Louis, MO).

Assessment of endotoxin contamination

BCP crystals were tested for lipopolysaccharide (LPS) contamination using the HEK-Blue^{TM} hTLR4 assay system (Invivogen). HEK-blue cells (5 x 10^5 cells/ml) expressing TLR4 were stimulated with LPS (1–100 ng/ml; positive control), or BCP crystals (50 ug/ml) for 24 hours. The expression of SEAP which is under the control of NF-κB and AP-1 was tested by incubating

cell supernatants with HEK-blue detection medium for 30 min at 37 °C and absorbance was read at 650 nm.

Supplementary Table 1: SYBR primer sequences

Gene	**Forward**	**Reverse**
HIF1a	5’ GAAACTTCTGGATGCTGGTGATTT 3’	5’ GCAATTCATCTGTGCTTTCATGTCA 3’
HIF2a	5’ AAGCTCCTCTCCTCAGTTTGCT 3’	5’ GTACAAGTTGTCCATCTGCTGG 3’
HK2	5’ TTCTTGTCTCAGATTGAGAGTGAC 3’	5’ TTGCAGGATGGCTCGGACTTG 3’
Glut1	5’ GAACTCTTCAGCCAGGGTCC 3’	5’ ACCACACAGTTGCTCCACAT 3’
PFKB3	5’ CCATGAAAGTCCGGAAGCAATG 3’	5’GCTTTTGACATCTCTCAAGGCAG3’
GAPDH	5’ ACAGTTGCCATGTAGACC 3’	5’ TTTTTGGTTGAGCACAGG 3’

Supplementary Table 2: Immunoblotting antibody dilutions

Primary antibody	**Dilution**	**Secondary antibody**	**Dilution**
Anti-Hexokinase 2	1:1000	Anti-mouse	1:3000
Anti-Glut1	1:1000	Anti-rabbit	1:2000
Anti-HIF1α	1:1000	Anti-mouse	1:2000
Anti-β-actin HRP	-	-	1:25,000

Supplementary Table 3: Seahorse calculations

Rate	**Calculation**
Basal Glycolysis	Average ECAR values prior to oligomycin treatment
Max Glycolysis	Average ECAR values after oligomycin and before FCCP
Glycolytic reserve	Max glycolysis-Basal glycolysis
Basal respiration	Average OCR values prior to oligomycin treatment –non-mitochondrial OCR
Max respiration	Average OCR values after FCCP & before Rotenone/antimycin A treatment
Respiratory reserve	Max respiration-basal respiration
Mitochondrial ATP production rate	OCR_{ATP} *2 *P/O
Glycolytic ATP production rate	PER-mitoPER
Total cellular ATP production rate	GlyoATP production rate + MitoATP production rate